Development of Advanced Electrochemical Emission Spectroscopy for Monitoring Corrosion in Simulated DOE Liquid Waste

Digby D. Macdonald (PI), Jun Liu (Ph. D., Graduated), Brian Marx (Grad. Assist.), Balaji Soundararajan (Grad. Assist.), Morgan Smith (Grad. Assist.), and Sejin Ahn (Grad. Assist. visiting from Korea).

Center for Electrochemical Science and Technology
Pennsylvania State University
University Park, PA 16802.

May 6-8 2003

Pacific Northwest National Laboratory
Richland, Washington.

OBJECTIVES

- **Develop a fundamental understanding of the corrosion and stress corrosion cracking of carbon steels in prototypical DOE liquid waste environments.**
- **Develop methods for deterministically predicting the accumulation of general and localized corrosion damage, including pitting attack and stress corrosion cracking, to liquid waste storage tanks.**
- **Optimize Electrochemical Emission Spectroscopy as a means of monitoring corrosion in DOE liquid waste storage tanks.**

Fundamental Understanding of Corrosion Processes

- **Understanding general corrosion in terms of the Point Defect Model, as revealed by Electrochemical Impedance Spectroscopy and Spectroscopic Ellipsometry.**
- **Characterizing the mechanism of passivity breakdown of nickel (a model system) as revealed by EIS and Mott-Schottky analysis.**
- **Detecting and characterizing individual micro fracture events in AISI 4340 steel at the crack tip.**

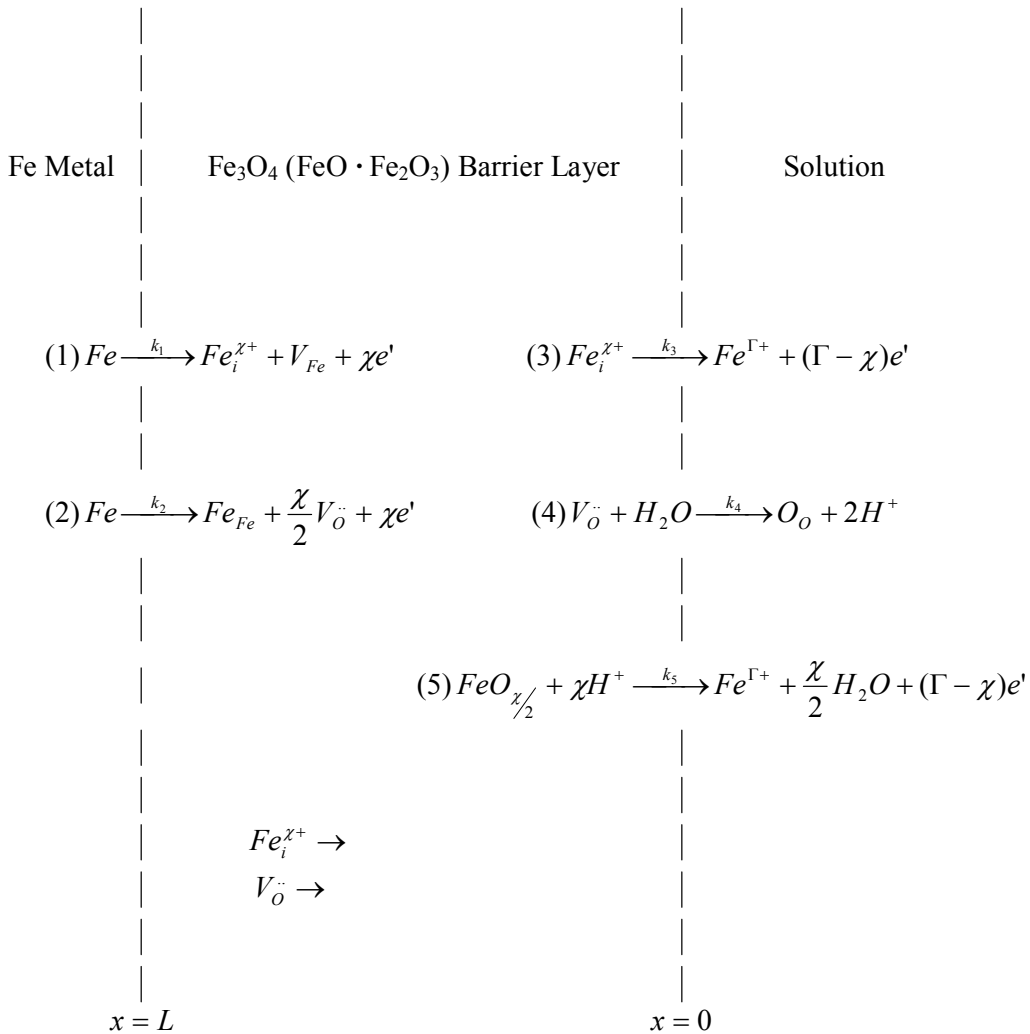

Figure 1. Schematic of physicochemical processes that occur within a barrier oxide (Fe_3O_4) layer on passive iron according to the Point Defect Model. Species include iron atoms; interstitial iron cations; iron vacancies in the metal phase; iron cations in a normal cation positions; iron cation in the solution phase; oxygen vacancies; and oxygen ions in anion sites in the film.

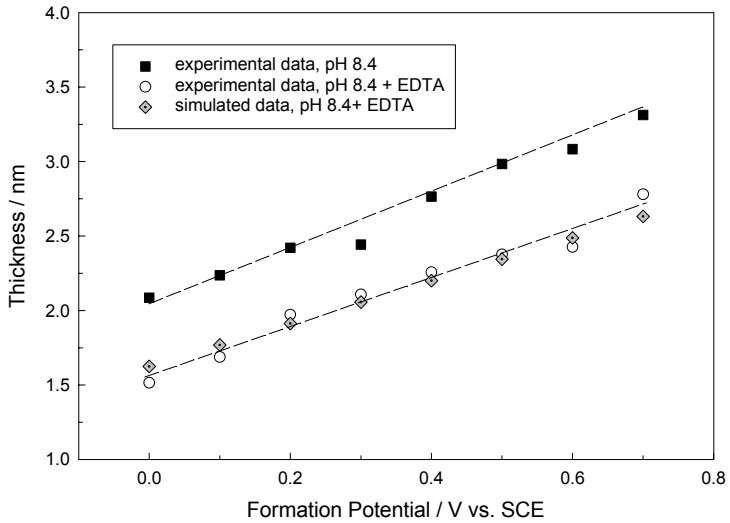

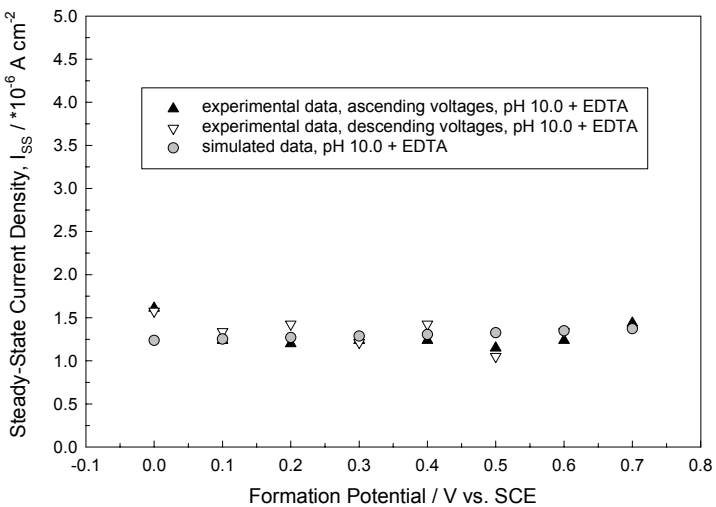

Figure 2. The steady-state film thickness (a) and current density (b) for the passive film on iron. Simulated data were calculated using fundamental parameters in the Point Defect Model.

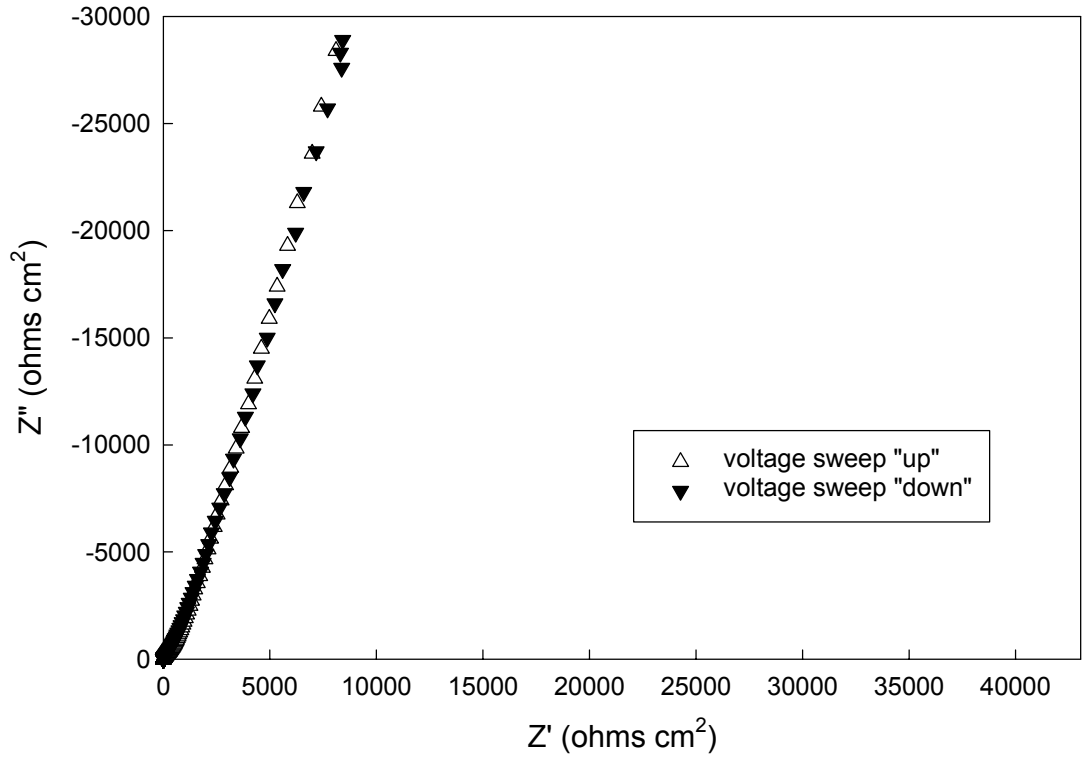

Figure 5. Nyquist plot for EIS data of the passive film formed on iron in borate buffer solution with 0.01 M EDTA (pH 8.15) at an applied film formation voltage of 0.2 V vs. SCE. Frequency range is from 10^4 Hz to 10^{-2} Hz. Perturbation voltage amplitude is 10 mV. Passive film formation voltage has been applied at 0.1, 0.2, 0.3, 0.4, 0.5, 0.6, 0.5, 0.4, 0.3, 0.2, 0.1 V vs. SCE continuously with a 24-hour polarization period for each voltage. "Up" means changing the formation voltage in the negative-to-positive direction; "down" in the positive-to-negative direction. "Up" and "down" voltage measurements have a time interval of 8 days in this case.

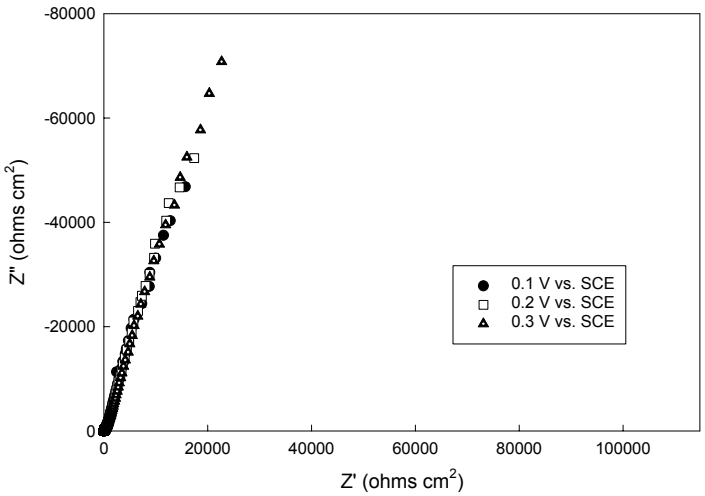

(a)

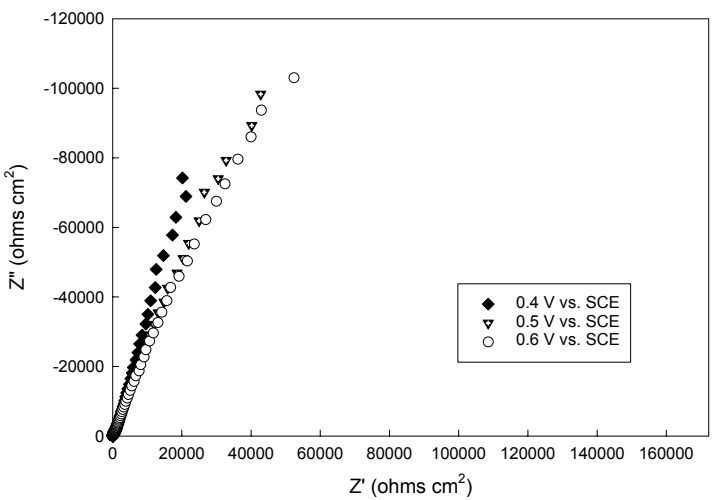

(b)

Figure 6. Nyquist plot for EIS data of the passive film formed on iron in borate buffer solution with 0.01 M EDTA (pH 10.05) as a function of formation voltage at a formation time of 24 hours. Spectra were measured using an excitation voltage of 10 mV and an applied frequency ranging from 10^4 Hz to 10^{-2} Hz.

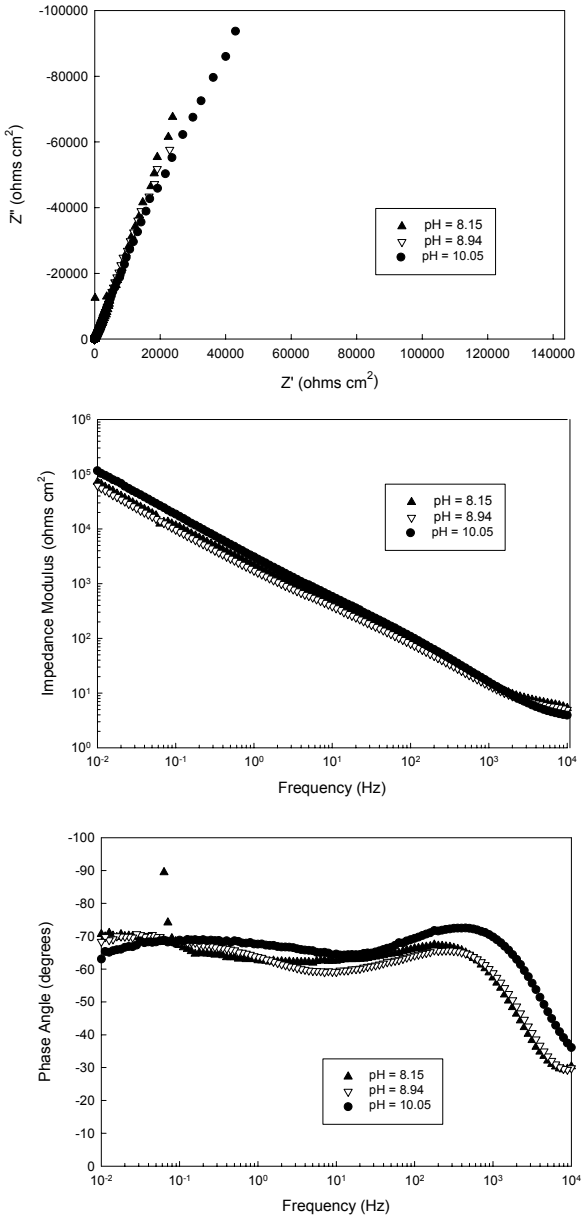

(a)

(b)

(c)

Figure 7. **Electrochemical impedance spectra for the passive film formed on iron in borate buffer / EDTA solution (formation voltage = 0.6 V vs. SCE) as a function of solution pH (pH = 8.15, 8.94, 10.05) at a formation time of 24 hours. Spectra were measured using an excitation voltage of 10 mV and an applied frequency ranging from 10^4 Hz to 10^{-2} Hz.**

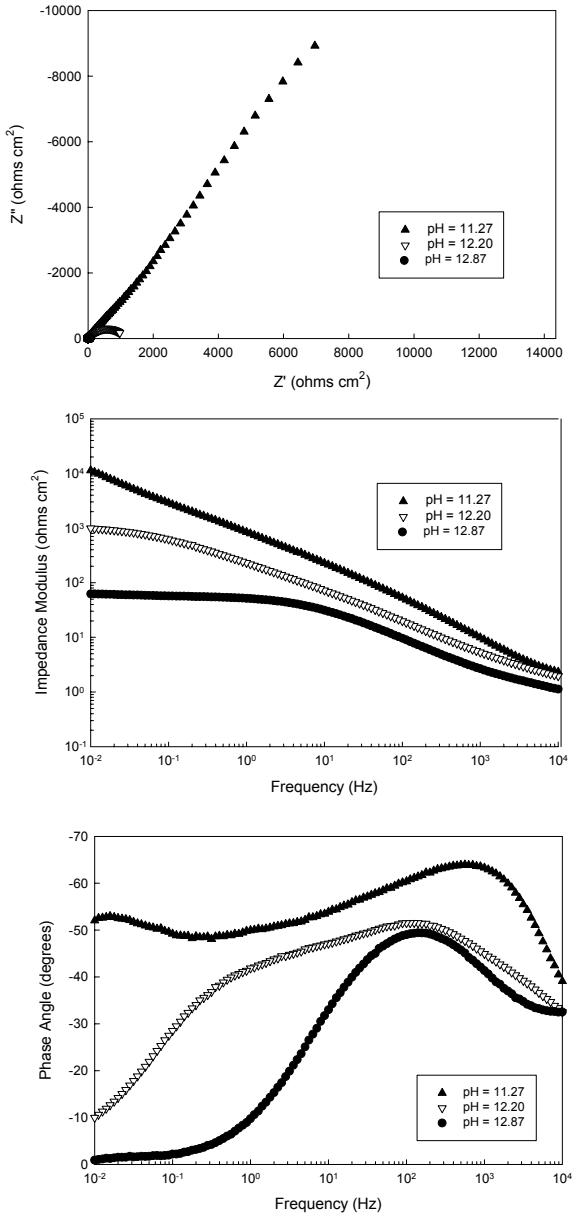

Figure 8. **Electrochemical impedance spectra for the passive film formed on iron in borate buffer / EDTA solution (formation voltage = 0.6 V vs. SCE) as a function of solution pH (pH = 11.27, 12.20, 12.87) at a formation time of 24 hours. Spectra were measured using an excitation voltage of 10 mV and an applied frequency ranging from 10^4 Hz to 10^{-2} Hz.**

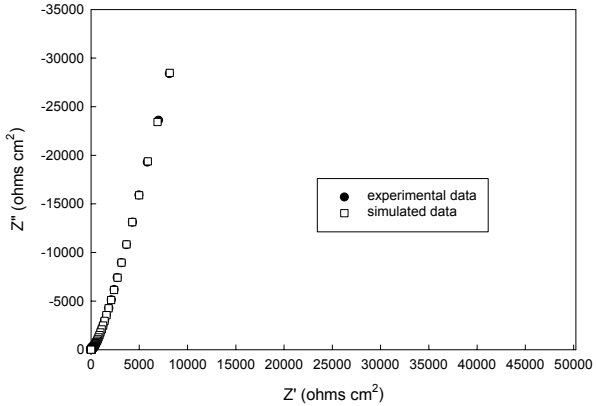

(a)

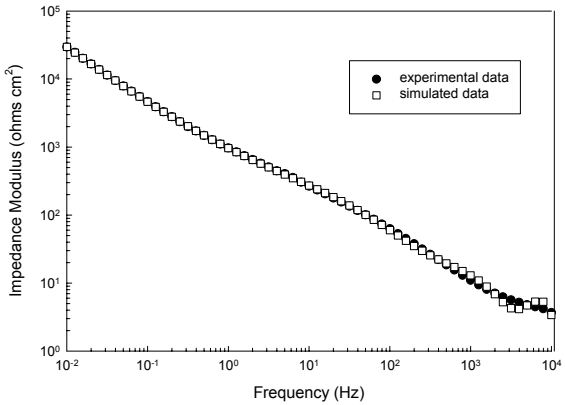

(b)

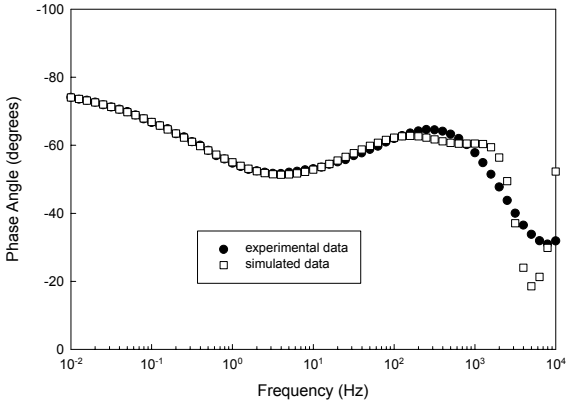

(c)

Figure 9. **Nyquist plot (a) and Bode plots (b, c) of impedance data for the passive film formed on iron in borate buffer solution with 0.01 M EDTA (pH 8.15) at an applied film formation voltage of 0.2 V vs. SCE. Closed circles represent experimental data and open squares represent simulated data using nonlinear fitted parameters.**

Model Parameter Values for Passive Iron in Alkaline Media

Transfer coefficients/ standard rate constants

$\alpha_1 = 0.01$ $\quad$ $k_1^{00} = 3.8\text{e-}12$ mol.cm^{-2}.s^{-1}

$\alpha_2 = 0.24$ $\quad$ $k_2^{00} = 1.1\text{e-}15$ mol.cm^{-2}.s^{-1}

$\alpha_3 = 0.39$ $\quad$ $k_3^{00} = 2.4\text{e-}6$ s^{-1}

$\alpha_5 = 0.30$ $\quad$ $k_5^{00} = 3.3\text{e-}8$ mol$^{0.4}$.cm$^{-0.2}$.s^{-1}

Potential distribution parameters

$\alpha = 0.728$

$\beta = -0.0047$

$\varepsilon = 1.10\text{e}6$ V/cm (Electric field strength)

$\varepsilon' = 30$ (Dielectric constant)

$\varphi_{f/s}^{0} = -0.29$ (Constant)

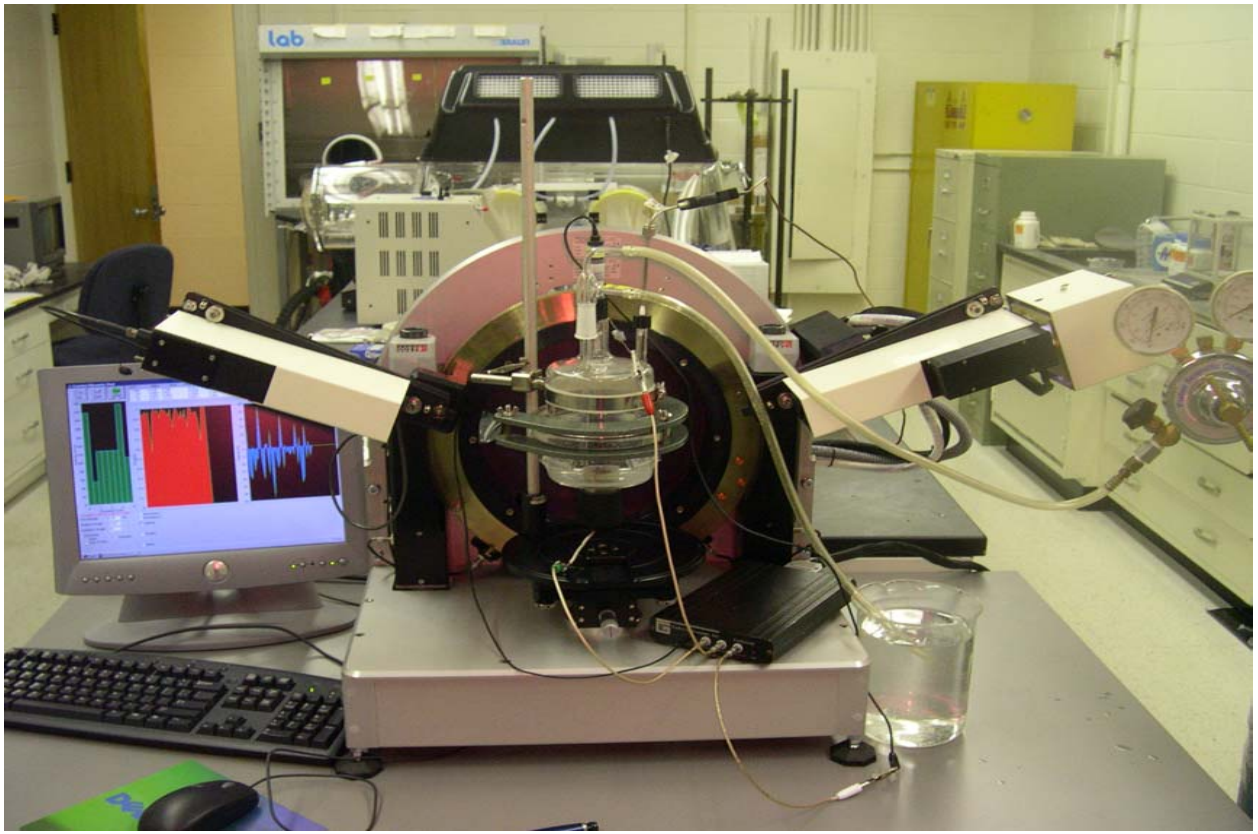

Figure 1. **Picture of the spectroscopic ellipsometer and associated systems. The PC used to collect the ellipsometric and impedance data (a). Two arms of ellipsometer-used to detect the changes in reflected light (b). Potentiostat/Frequency Response Analyzer (FRA) for controlling the potential at the working electrode and measuring AC impedance (c) . The cell containing the electrochemical set-up (d) .**

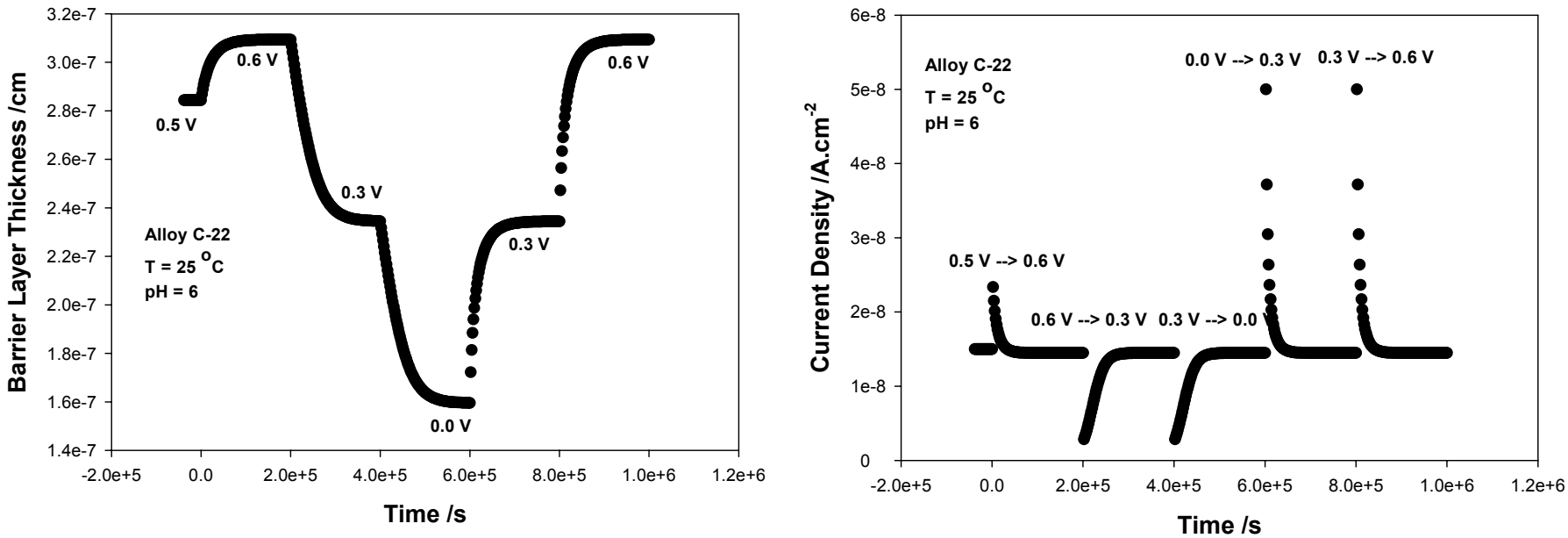

Figure 4. **Calculated transients in the barrier layer thickness and anodic (passive) current density for Alloy C-22 upon stepping the potential in the negative and positive directions. Alloy C-22, T = 25 °C, pH = 6. Voltages are with respect to the Standard Hydrogen Electrode (she).**

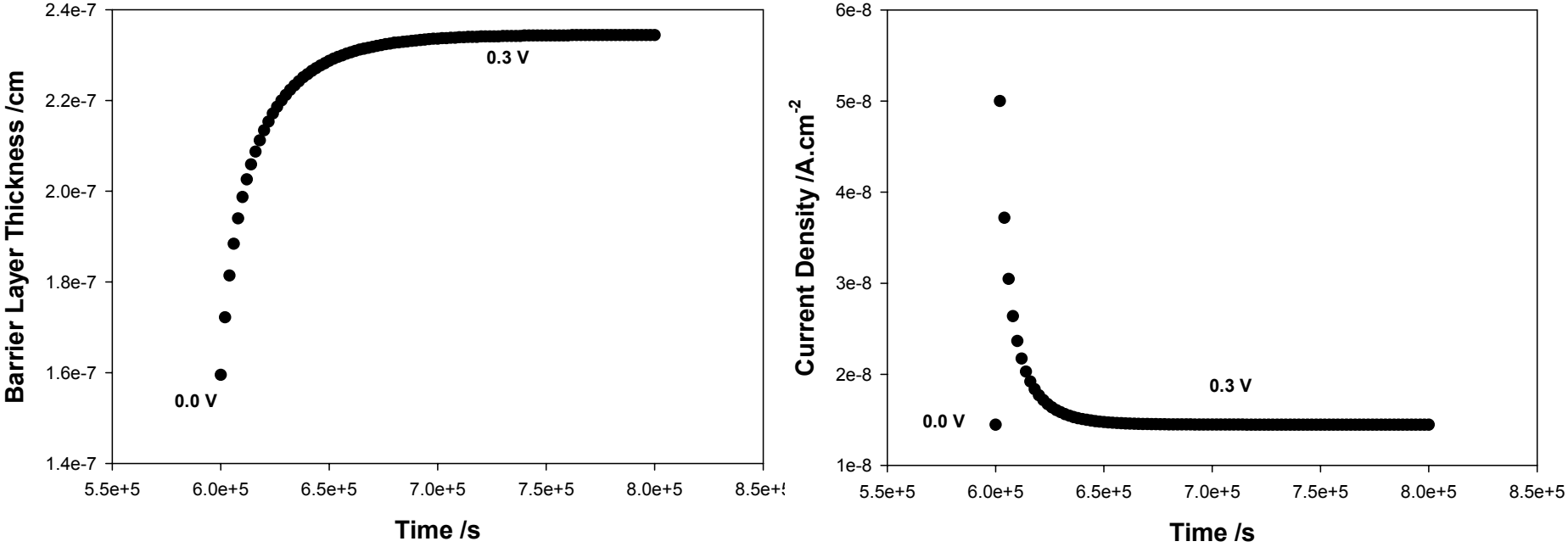

Figure 5. Transients in the barrier layer thickness and current density for a step decrease in potential from 0.6 V_{she} to 0.3 V_{she} for Alloy C-22, T = 25 ^{o}C, pH = 6.

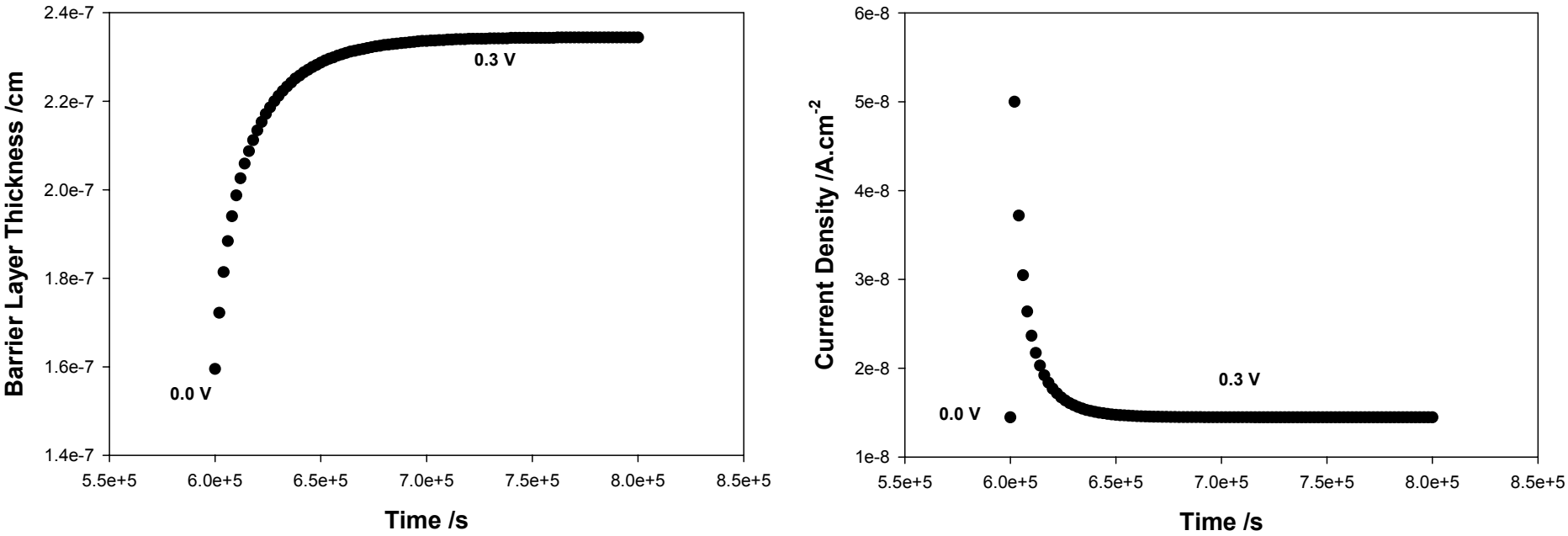

Figure 6. Transients in the barrier layer thickness and current density for a step decrease in potential from 0.0 V_{she} to 0.3 V_{she} for Alloy C-22, T = 25 ^{o}C, pH = 6.

Findings

- **Growth of the passive film on iron in alkaline solutions is well-described by the Point Defect Model.**
- **Barrier layer of the passive film on iron is an n-type semi-conductor, in which the donors are oxygen vacancies or metal interstitials, or both.**
- **Electrochemical Impedance Spectroscopy is a powerful and convenient means of extracting model parameters.**
- **Passivity breakdown on nickel in chloride-containing solutions is also well-described by the Point Defect Model. The role of chloride ion is to catalyze the generation of cation vacancies at the barrier layer/solution interface, resulting in a steady increase in the concentration of cation vacancies in the film and ultimately in the condensation of vacancies at the metal/barrier layer interface.**

Passivity Breakdown

- **Responsible for localized corrosion, including pitting corrosion and stress corrosion cracking.**
- **Point Defect Model postulates that passivity breakdown is caused by the condensation of cation vacancies at the metal/passive film interface (see next slide).**
- **Nickel selected as the model system, because the NiO passive film is p-type in electronic character and hence contains an excess of cation vacancies.**
- **By using Mott-Schottky analysis, we can measure the concentration of cation vacancies in the film and hence determine the change in their concentration in response to an environmental stress.**

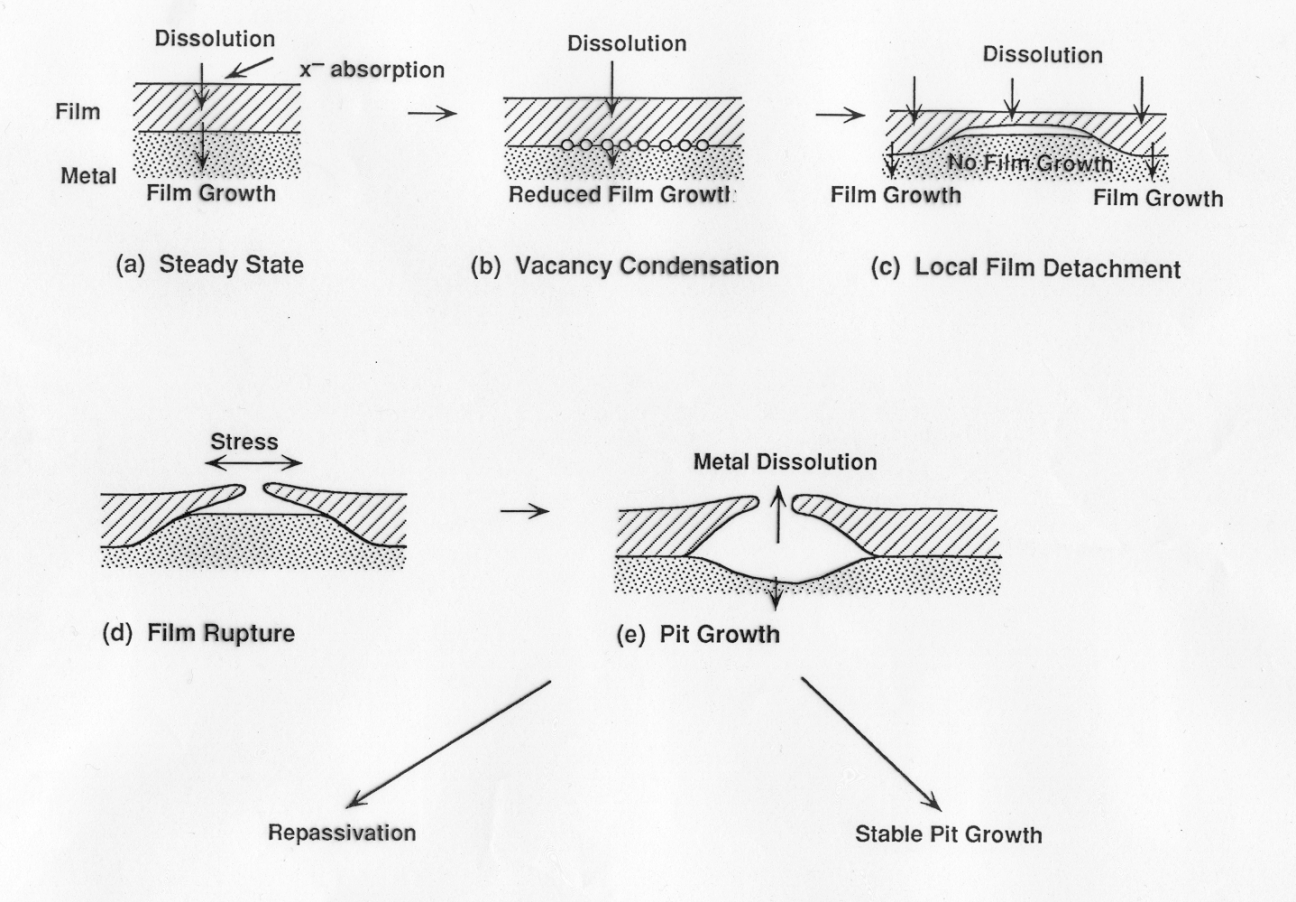

Figure 2. Cartoon outlining various stages of pit nucleation according to the Point Defect Model.

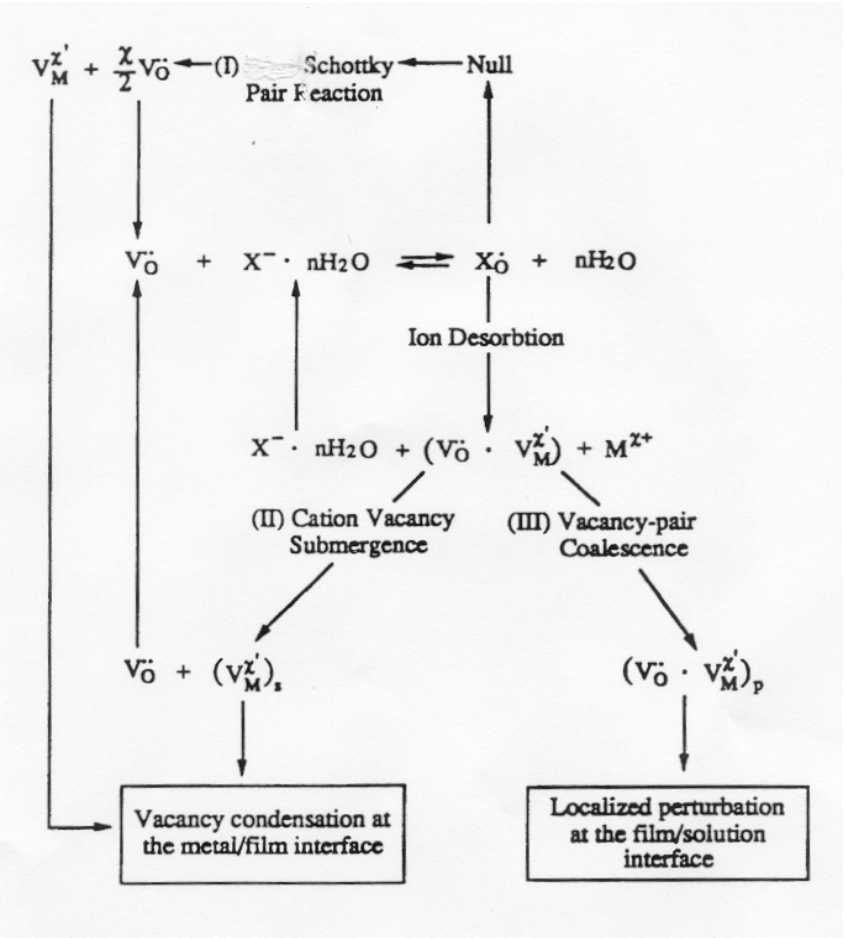

Figure 3. Postulated reactions for cation vacancy generation at the barrier layer/solution interface according to the Point Defect Model.

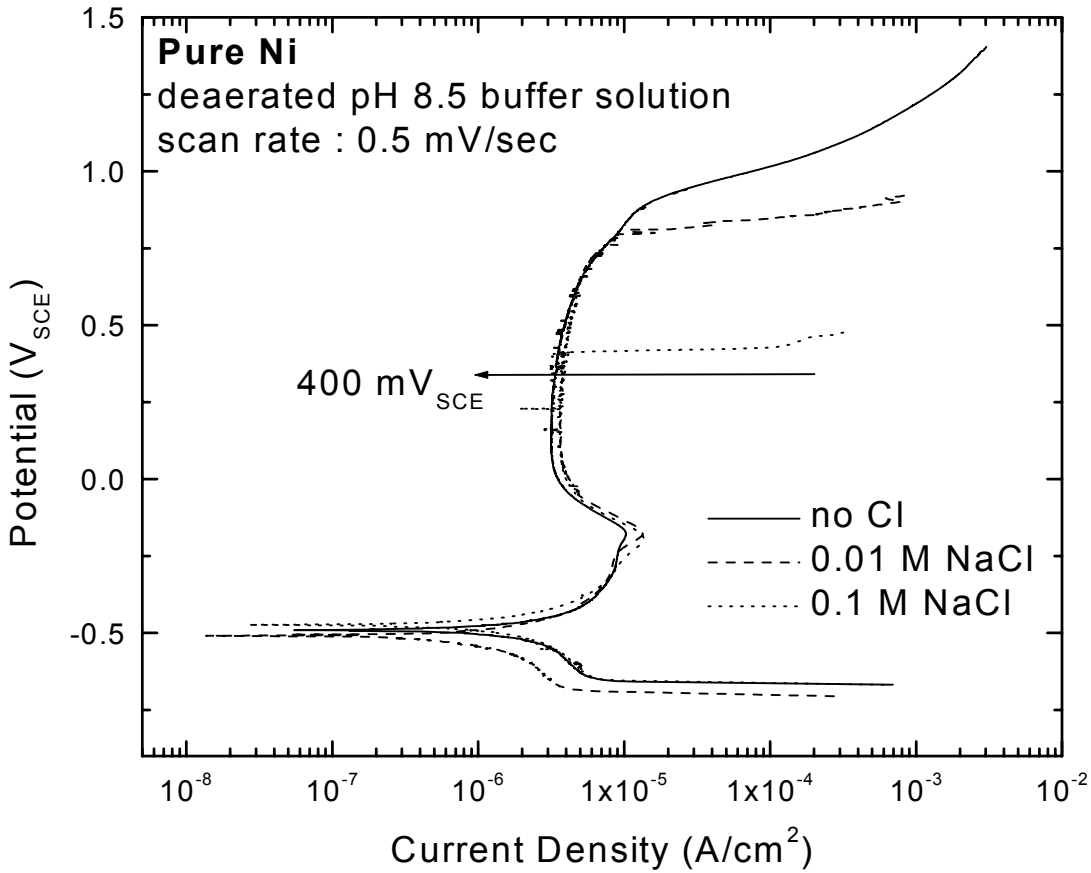

Figure 4. Polarization curves for nickel in borate buffer solution with or without chloride ion.

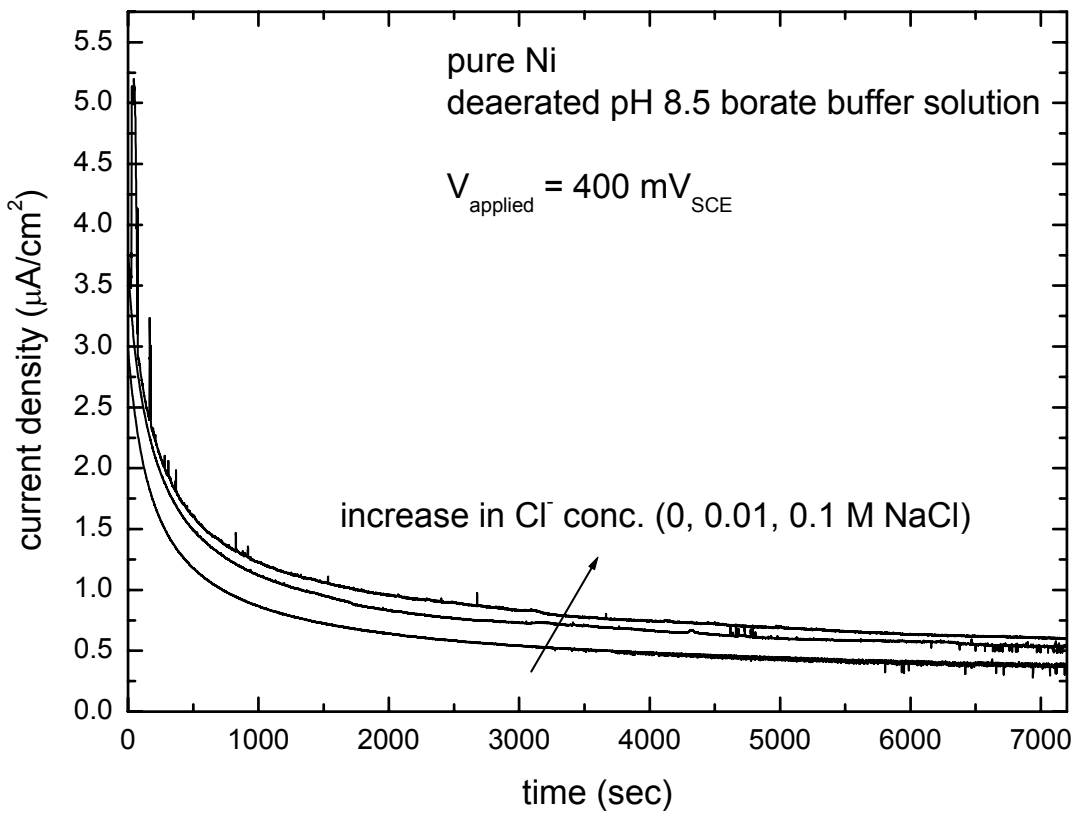

Figure 5. Current transients for Ni in Cl^- containing, deaerated pH 8.5 borate buffer solutions measured at 400 mV_{SCE}. The concentration of Cl^- was controlled from 0 to 0.1 M by adding NaCl to the solution.

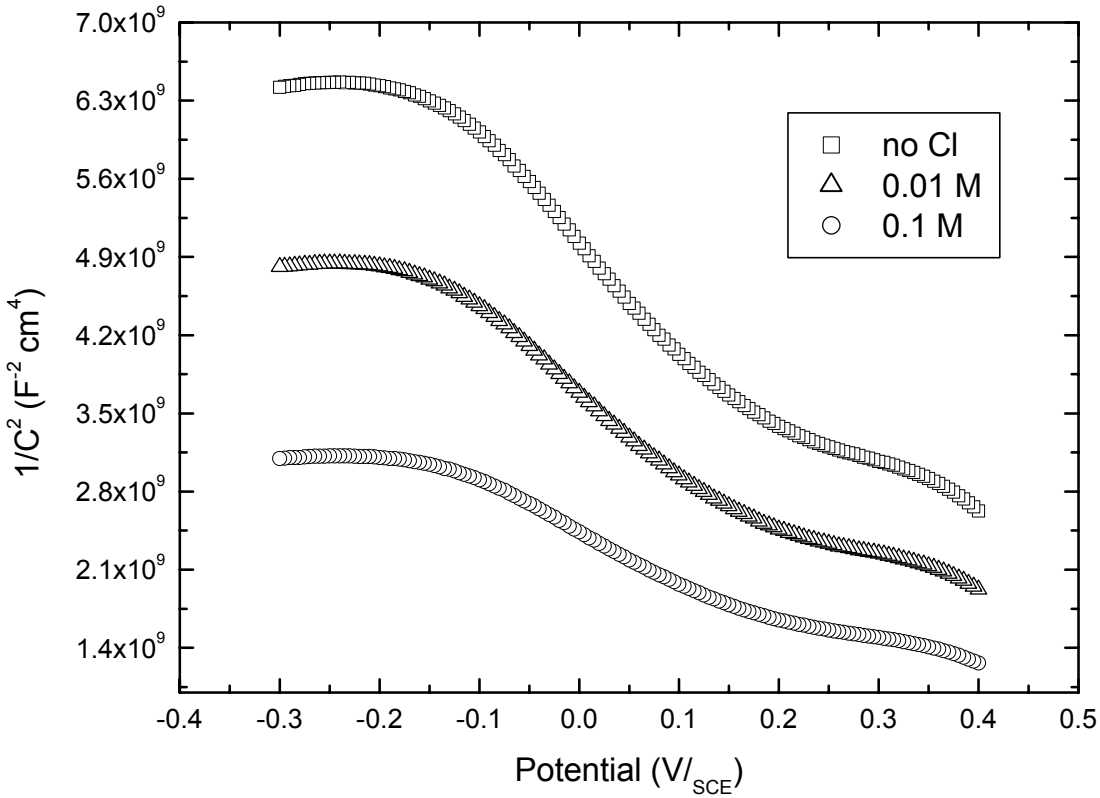

Figure 6. Mott-Schottky plots for the passive film formed on Ni in deaerated pH 8.5 borate buffer solution at 400 mV_{SCE} for 2 hours with different concentration of Cl^- ions measured at a frequency of 1 kHz.

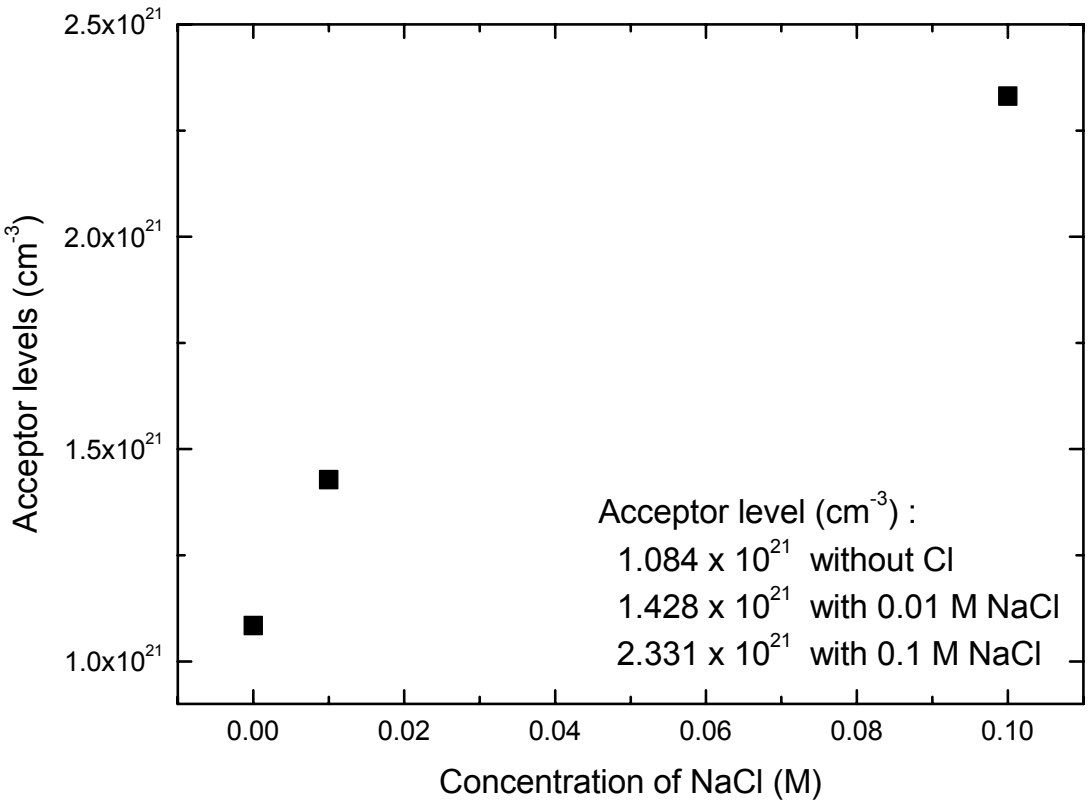

Figure 7. Acceptor levels calculated from the slopes of plots in Fig. 6.

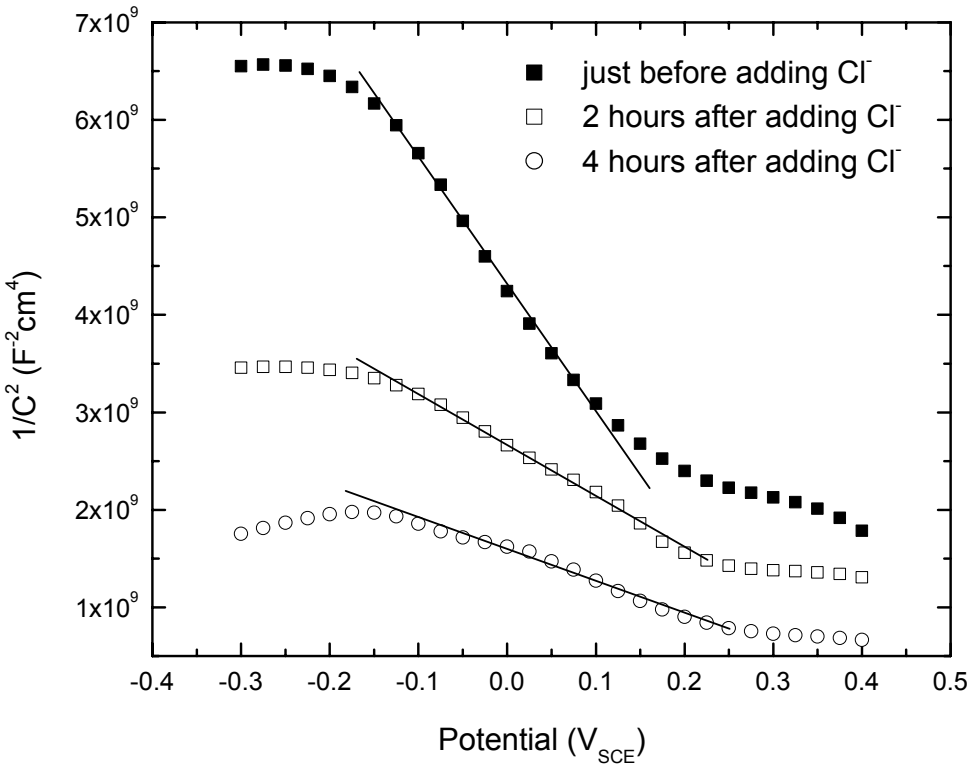

Figure 8. Mott-Schottky plots for the passive film formed on Ni in deaerated pH 8.5 borate buffer solution at 400 mV_{SCE} at a frequency of 1 kHz. The passive film was initially grown in Cl^-free solution for 2 hours and then NaCl was added to the solution to adjust the total concentration of Cl^- ions in the solution to 0.1 M.

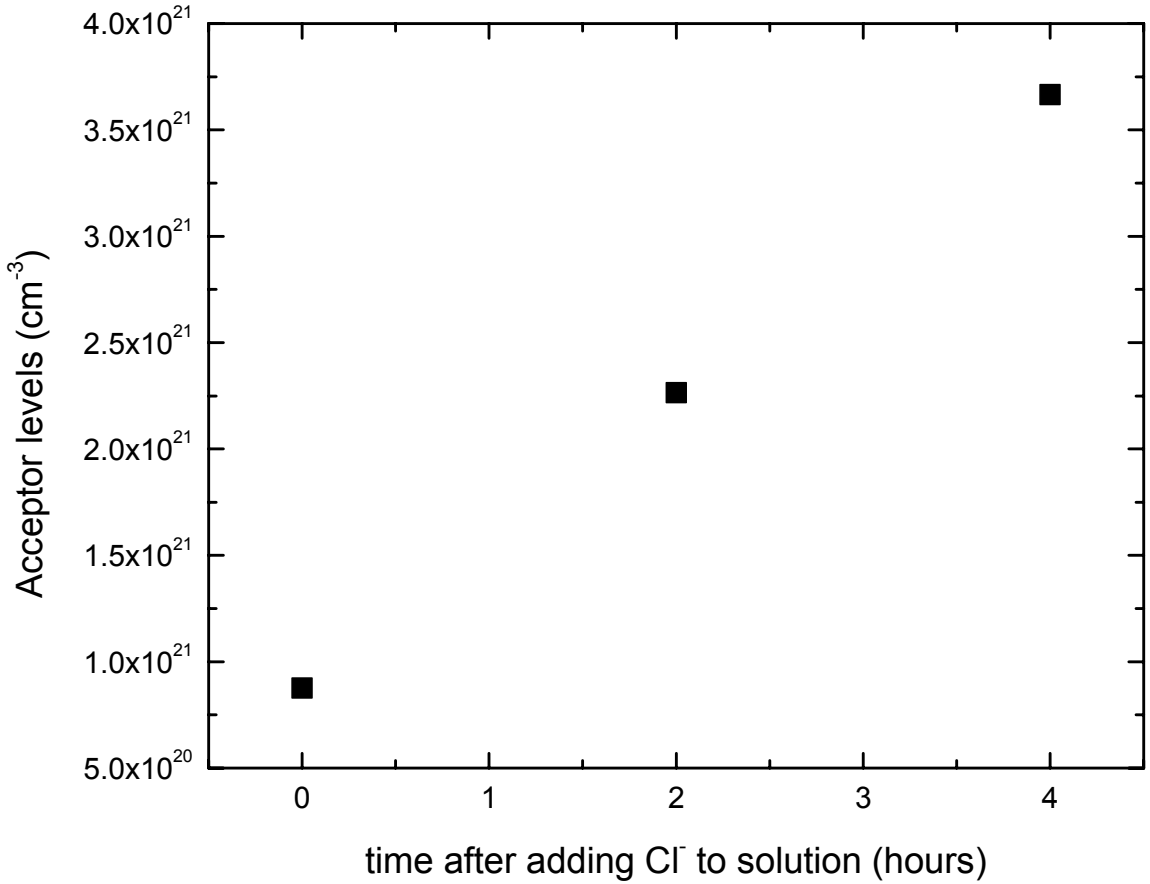

Figure 9. Acceptor levels calculated from the slopes of plots in Fig. 8.

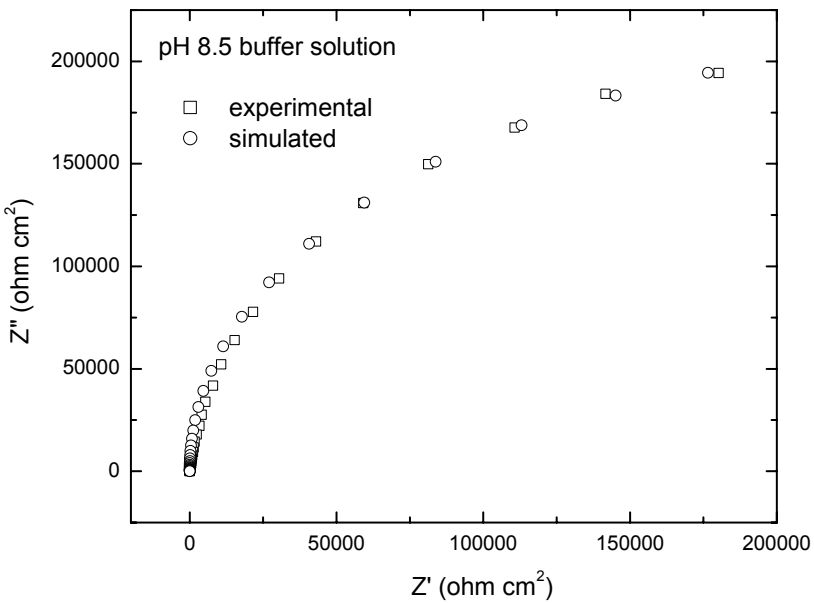

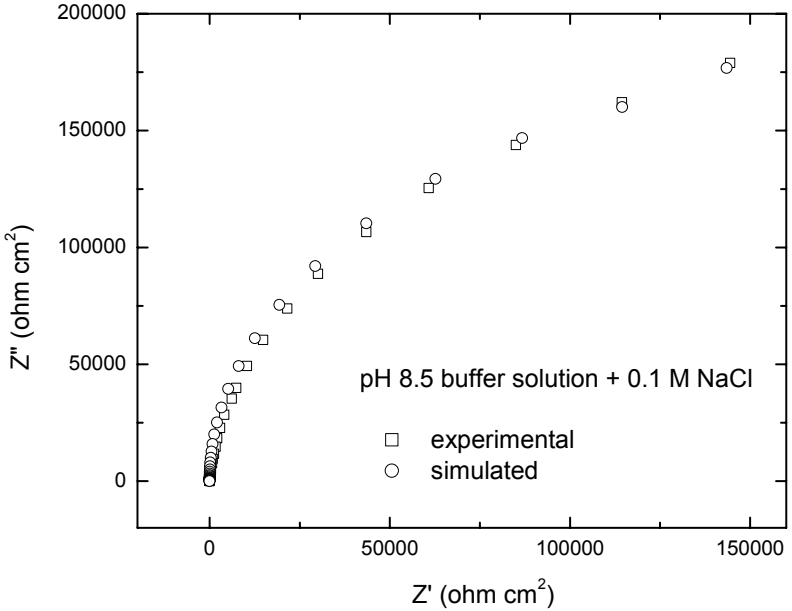

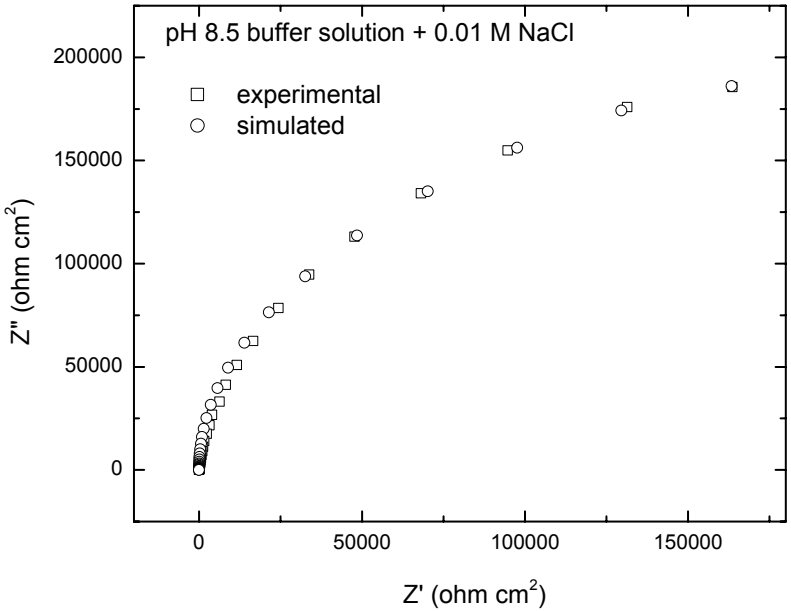

Figure 10. Nyquist plots for the passive film formed on Ni in Cl^- containing, pH 8.5 borate buffer solutions at 400 mV_{SCE} for 2 hours together with the model fit by the PDM. The concentration of Cl^- ions in the solution was (a) 0 M, (b) 0.01 M and (c) 0.1 M.

Table 1. Values for a partial list of parameters in the Point Defect Model as determined by fitting the PDM to the experimental electrochemical impedance data.

Parameter	0 M NaCl	0.01 M NaCl	0.1 M NaCl
Electric Field Strength $\hat{\varepsilon}$ *(V/cm)*	1.00×10^{6}	1.00×10^{6}	1.00×10^{6}
Rate Constant, k_1^{00} *(cm/s)*	2.306×10^{-12}	3.190×10^{-12}	3.422×10^{-12}
Rate Constant, k_3^{00} *(mol/cm*^{2}*s)*	2.895×10^{-18}	3.112×10^{-18}	3.035×10^{-18}
Rate Constant, k_4^{00} *(mol/cm*^{2}*s)*	4.926×10^{-14}	3.908×10^{-13}	6.392×10^{-12}
Rate Constant, k_7^{00} *(mol*$^{0.4}$*/cm*$^{0.2}$*s)*	3.000×10^{-12}	3.633×10^{-12}	3.604×10^{-12}
Transfer Coeff., ? $_?$	0.405	0.398	0.384
Transfer Coeff., ? $_?$	0.077	0.078	0.076
Transfer Coeff., ? $_?$	0.192	0.056	0.099

Findings

- **Passivity breakdown on nickel is well-described by the Point Defect Model.**
- **The data are inconsistent with the chloride-catalyzed dissolution or the chloride penetration models.**
- **PDM is assumed then to apply to iron, because of similarities in the dependencies of the breakdown voltage and the induction time on system independent variables ([Cl-], pH, potential).**
- **Now in a position to apply Damage Function Analysis to the deterministic prediction of pitting damage to iron in simulated DOE liquid waste storage tanks.**

Stress Corrosion Cracking

- **Caustic cracking of hard, heat-affected zones adjacent to welds in liquid waste storage tanks is a continual threat to tank integrity.**
- **Little mechanistic detail is known of caustic cracking of high strength steels, other than it appears to be due to "hydrogen embrittlement".**
- **Mechanistic details must be resolved before effective mitigation techniques can be developed.**

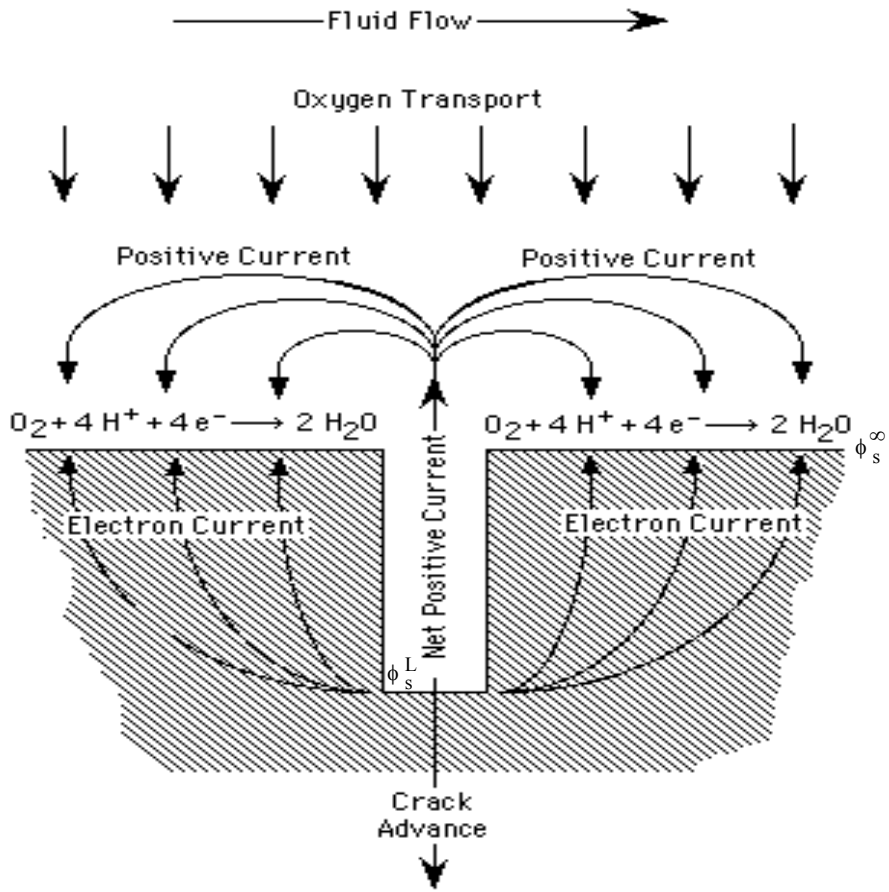

Figure 1. Schematic of the origin of the coupling current in stress corrosion cracking. The coupling current is required by the differential aeration hypothesis for localized corrosion and the conservation of charge requires that the electron current flowing through the substrate from the crack to the external surface must be equal to the positive ionic current flowing through the solution from the crack to the external surface.

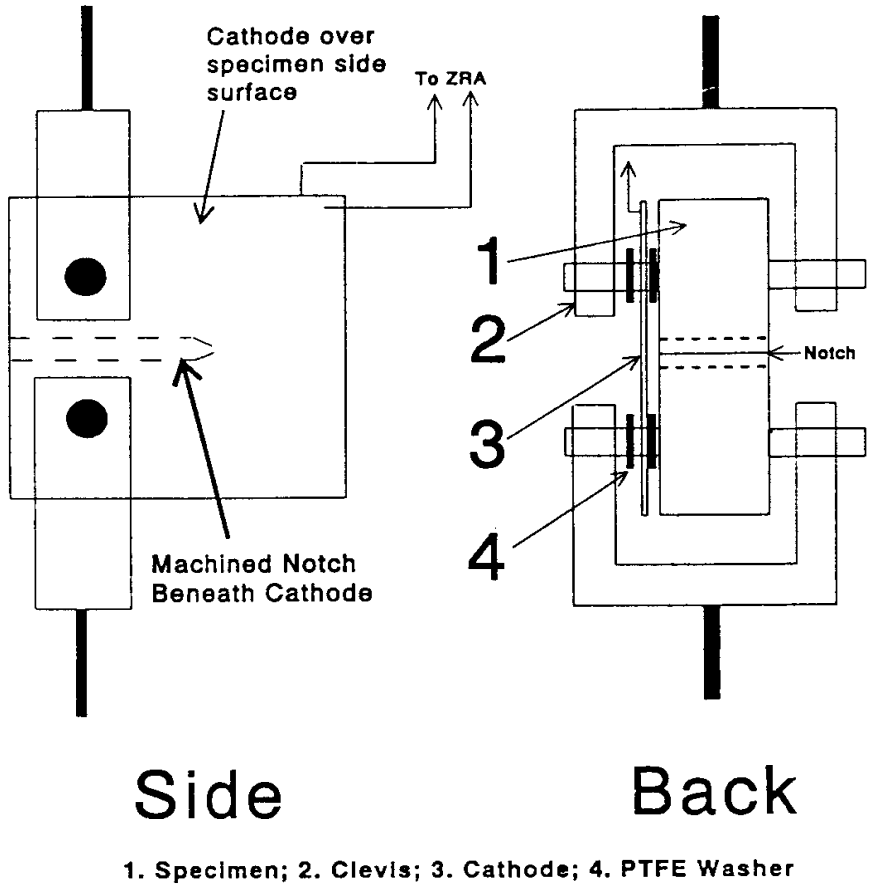

Figure 2. **Specimen configuration used in detecting and measuring the coupling current flowing from a crack to the external metal surface. Note that the C(T) fracture mechanics specimen is coated with PTFE to inhibit the cathodic reduction of oxygen on the specimen surface. Instead, the current flows from the crack to the side cathodes (only one shown) where it is consumed by O_2 reduction. The electron current flows from the crack tip to the side cathodes via a zero resistance ammeter, which is used for its measurement**

Figure 3. The experimental cell loaded on the tensile testing machine for measuring the coupling current that flows from the crack to the external surfaces during stress corrosion cracking in AISI 4340 steel in caustic solution.

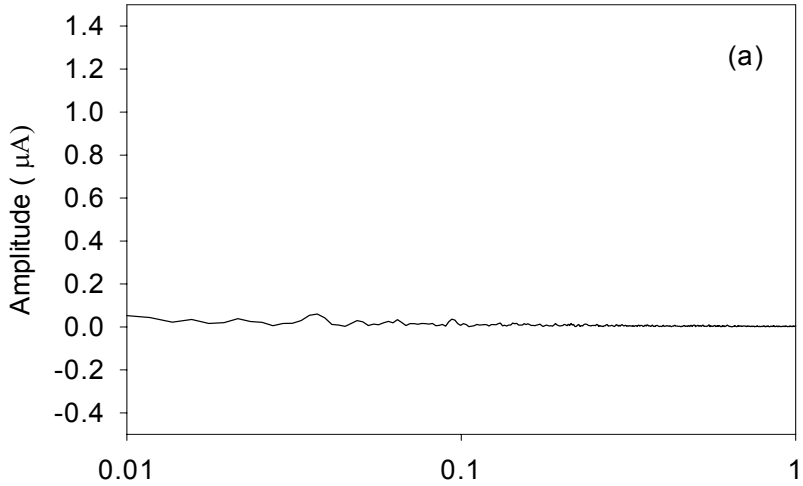

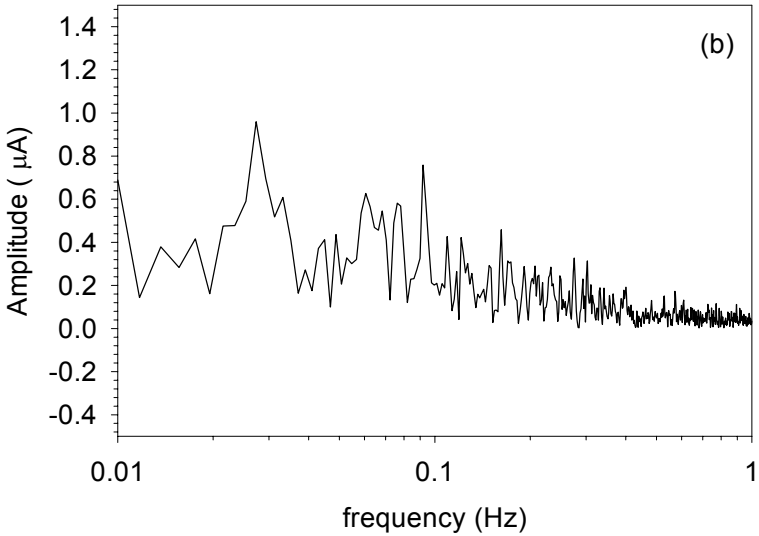

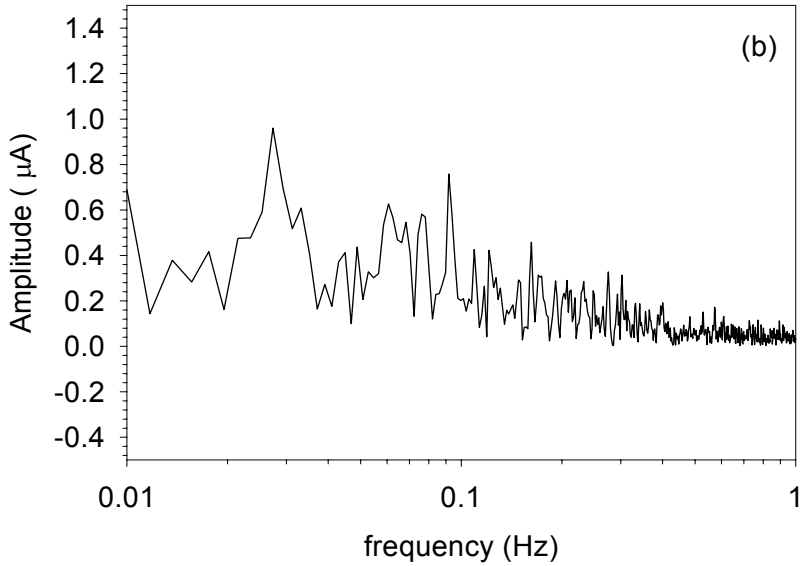

Figure 6. Amplitude vs. frequency after FFT transformation of the (electron) coupling current for AISI 4340 steel in 12 M NaOH solution at 70 °C. (a) Before loading application; (b) during the second stage of fracture; and (c) before final fracture of the specimen.

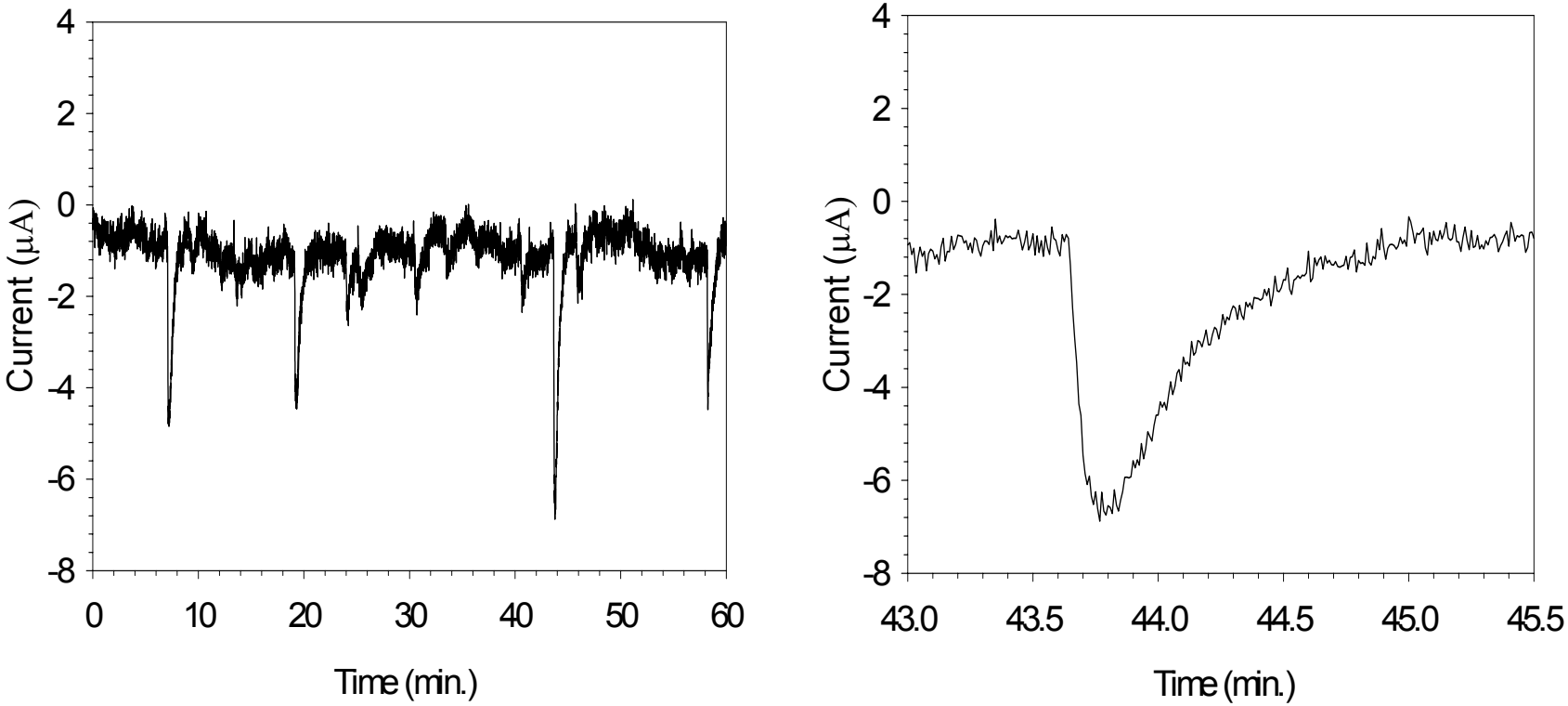

Figure 4. Transient in coupling current due to the occurrence of a micro fracture event at the tip of a crack in AISI 4240 steel in 6 M NaOH solution at 70 °C. Note the sharp shift of the current in the negative direction upon initiation of the fracture event, corresponding to brittle fracture, followed by a slow relaxation as the freshly generated metal surfaces passivated.

Micro Fracture Event Dimension

Finally, assuming that the fracture events are semi-circular in geometry of radius *r* and that the frequency at which they occur is *f*, the crack growth rate can be written as[2]

$$\frac{dL}{dt} = \frac{2r^2 f}{B_n} \tag{1}$$

where B_n is the specimen thickness at the groove. Equation (1) is readily rearranged to yield the micro fracture dimension as

$$r = \sqrt{\frac{B_n . dL/dt}{2f}} \tag{2}$$

For the 6 M NaOH case, dL/dt = 5.3 x 10^{-8} cm/s, B_n = 2.7 cm, and $f \approx 0.003$ s^{-1}, yielding a micro fracture dimension of ≈ 49 μm. Note that the fracture frequency is somewhat subjective, because it depends upon what is counted as a "fracture event". In the present case, eleven events were counted over the sixty minutes recorded in Figure 11, resulting in the value given above for *f*. The calculated fracture dimension may be compared with the 3 μm dimension found for the fracture of sensitized Type 304 SS in high temperature water[2]. It is likely, however, that larger micro fracture events give rise to the more intense current transients, so that the 49 μm dimension estimated above probably represents the upper end of a distribution in this quantity. Because the dimension of a slip event should be a small multiple of the Burger's vector (nanometers), the fracture dimension appears to be much too large to be consistent with the slip/dissolution/repassivation mechanism for crack advance. On the other hand, the dimension is consistent with a hydrogen embrittlement mechanism.

First Order Kinetic Plot, $Ln(I/I_o)$ vs ΔT

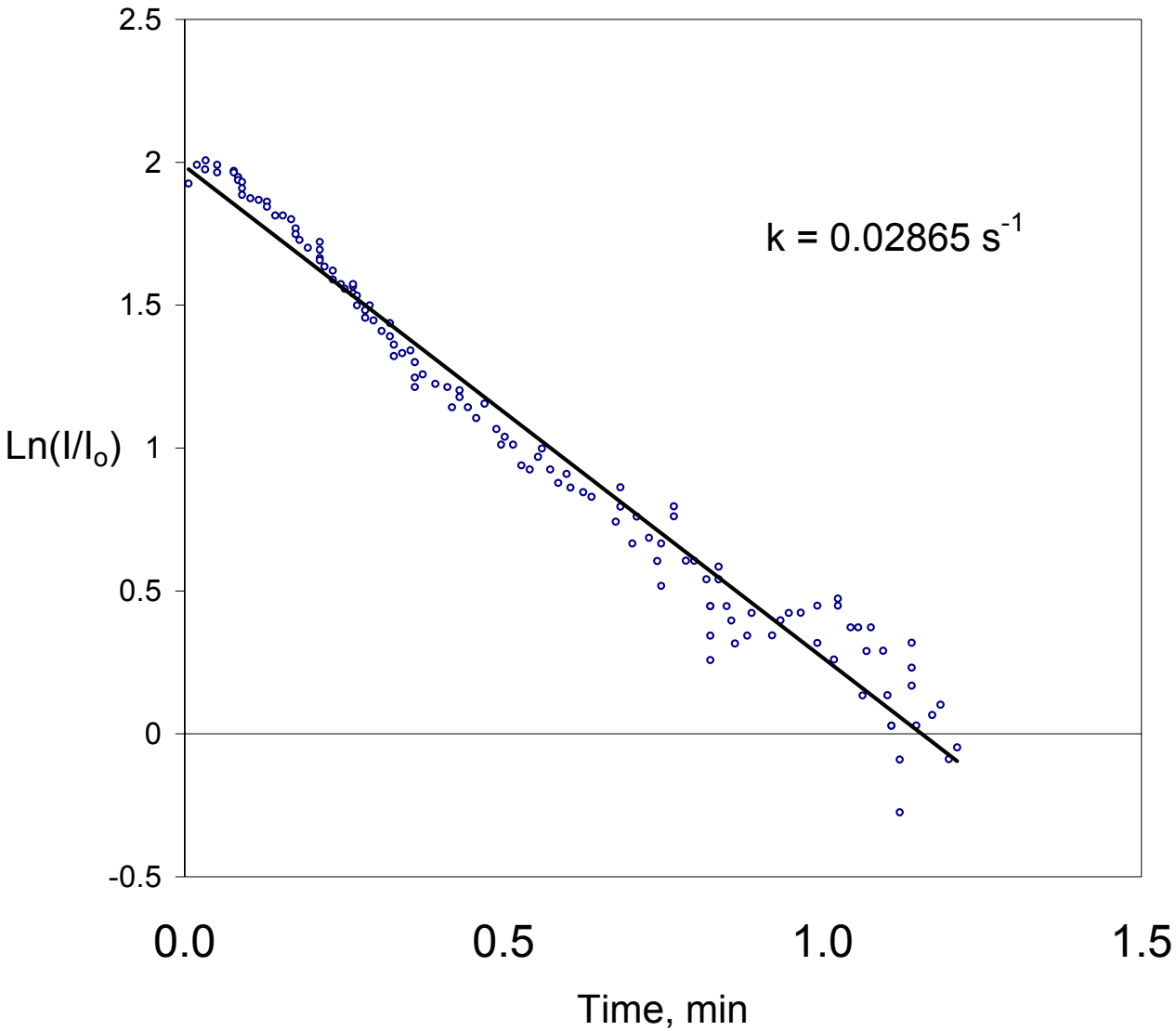

Findings

- **First electrochemical characterization of micro fracture events in any system under free corrosion conditions.**
- **Caustic cracking in AISI 4340 steel is due to hydrogen embrittlement, as judged by the dimension of the micro fracture event.**
- **First determination of the kinetics of repassivation of a micro fracture event at a crack tip.**

Future Work

- **Develop a comprehensive database of PDM parameter values for iron in alkaline solutions at temperatures ranging from 25 ^{o}C to 95 ^{o}C.**
- **Continue to explore the mechanisms of passivity breakdown and caustic cracking of carbon steel in alkaline solutions.**
- **Customize Damage Function Analysis to DOE liquid waste tanks in order to predict the accumulation of general and localized corrosion damage.**
- **Further develop EES (electrochemical noise) as a means of monitoring corrosion damage in the storage tanks. Work will emphasize wavelet analysis, because it promises to allow differentiation between various forms of localized corrosion from the recorded noise.**